Characterization of Dihydro-A2PE: An Intermediate in the A2E Biosynthetic Pathway†

So R. Kim,‡ Jiangtao He,|| Emiko Yanase,‡,|| Young P. Jang,‡ Nina Berova,|| Janet R. Sparrow,*,‡,§ and Koji Nakanishi*,||

Departments of Ophthalmology, Pathology and Cell Biology, and Chemistry, Columbia University, New York, New York 10032

Received May 19, 2007; Revised Manuscript Received June 26, 2007

ABSTRACT: Bisretinoid lipofuscin pigments that accumulate in retinal pigment epithelial cells are implicated in the etiology of several forms of macular degeneration, including juvenile onset Stargardt disease, Best vitelliform macular degeneration, and age-related macular degeneration. One of these compounds, A2E, is generated by phosphate hydrolysis of a phosphatidyl-pyridinium bisretinoid (A2PE) that forms within photoreceptor outer segments. Here, we demonstrate that the formation of the aromatic pyridinium ring of A2PE follows from the oxidation of a dihydropyridinium intermediate. Time-dependent density functional theory calculation, based on the structure of dihydro-A2E, produced a simulated UV−visible absorbance spectrum characterized by maxima of 494 and 344 nm. Subsequently, a compound exhibiting similar UV−visible absorbance maxima (λ_{max} 490 and 330 nm) was identified in the A2E biomimetic reaction mixture. By liquid chromatography−mass spectrometry (LC-MS) this bischromophore had the expected mass of the dihydro-pyridinium bisretinoid. The compound also exhibited the behavior of a biosynthetic intermediate since it formed in advance of the final product A2E and was consumed as A2E accumulated. Moreover, under deoxygenated conditions, conversion to the aromatic pyridinium bisretinoid was inhibited. Taken together, these findings indicate that A2E biosynthesis involves the oxidation of a dihydropyridinium intermediate dihydro-A2PE. An understanding of the biosynthetic pathways of retinal pigment epithelial lipofuscin pigments is critical to the development of therapies for macular degeneration that are based on limiting the formation of these damaging compounds.

A number of observations over the years have shown that the deposition of lipofuscin fluorophores in retinal pigment epithelium (RPE[1]) is dependent on the availability of vitamin A and/or vitamin A derivatives. For instance, *Rpe65* null mutation (*1*), amino acid variants in *Rpe65* (*2*), antagonists of RPE65 (*3*), and retinoids (13-*cis*-retinoic acid) that inhibit 11-*cis*-retinol dehydrogenase (*4*, *5*), all of which slow the visual cycle and reduce the flux of all-*trans*-retinal, also limit the formation of RPE lipofuscin. In addition, RPE lipofuscin accumulation in normal rat retina can be reduced by dietary vitamin A deficiency (*6*, *7*), while pharmacological agents that reduce serum vitamin A also decrease RPE lipofuscin in mice (*8*).

The first of the vitamin A aldehyde derivatives to be identified in RPE lipofuscin was A2E (Figure 1), a pyridinium bisretinoid conjugate (*9*−*12*) ($C_{42}H_{58}NO$, molecular weight 592), named because it can be synthesized biomimetically from vitamin A aldehyde and ethanolamine when combined in a 2:1 ratio. Later, a C13−C14 *Z*-isomer of A2E (isoA2E) (Figure 1) was identified (*12*), along with minor isomers having *cis* double bonds at other positions (*13*). Confirmation of the structure of A2E was obtained by extensive nuclear magnetic resonance (NMR) studies (*12*) and by total synthesis (*14*). Other constituents of RPE lipofuscin include pigments generated via the condensation of two all-*trans*-retinal (*15*, *16*). These compounds include an all-*trans*-retinal dimer (atRAL dimer) and the conjugates all-*trans*-retinal dimer-phosphatidylethanolamine (atRAL dimer-PE) and all-*trans*-retinal dimer-ethanolamine (atRAL dimer-E).

We previously proposed an A2E biosynthetic cascade (*12*, *17*) (Figure 1) that is initiated with a reaction between the membrane phospholipid phosphatidylethanolamine (PE) and all-*trans*-retinal, the latter being generated upon photoisomerization of 11-*cis*-retinal (Figure 1). We demonstrated by mass spectrometry analysis (*17*) that the compound formed by this reaction is the Schiff base conjugate, *N*-retinylidene-phosphatidyl-ethanolamine (NRPE), while others showed that

† These studies were funded by National Institutes of Health Grant EY 12951 (J.R.S.) and GM 36564 (K.N. and N.B.), the Steinbach Fund, Research to Prevent Blindness, and the Kaplen Fund. J.R.S. is a recipient of an Alcon Research Institute Award.

* To whom correspondence should be addressed. For J.R.S.: 630 W. 168th Street, New York, NY 10032. Phone: (212) 305-9944. Fax: (212) 305-9638. E-mail: jrs88@columbia.edu. For K.N.: 3000 Broadway, New York, NY 10027. E-mail: kn5@columbia.edu.

‡ Department of Ophthalmology.

§ Department of Pathology and Cell Biology.

|| Department of Chemistry.

[1] Abbreviations: AMD, age-related macular degeneration; atRAL dimer-E, all-*trans*-retinal dimer-ethanolamine; atRAL dimer-PE, all-*trans*-retinal dimer-phosphatidylethanolamine; DP-dihydro-A2PE, dipalmitoyl-dihydro-A2PE; DPBS, Dulbecco's phosphate buffered saline; HPLC, high performance liquid chromatography; LC-MS, liquid chromatography−mass spectrometry; NMR, nuclear magnetic resonance; NRPE, *N*-retinylidene-phosphatidyl-ethanolamine; PE, phosphatidylethanolamine; PLD, phospholipase D; RPE, retinal pigment epithelium; TDDFT, time-dependent density functional theory; TFA, trifluoroacetic acid.

10.1021/bi7009635 CCC: $37.00
Published on Web 08/08/2007

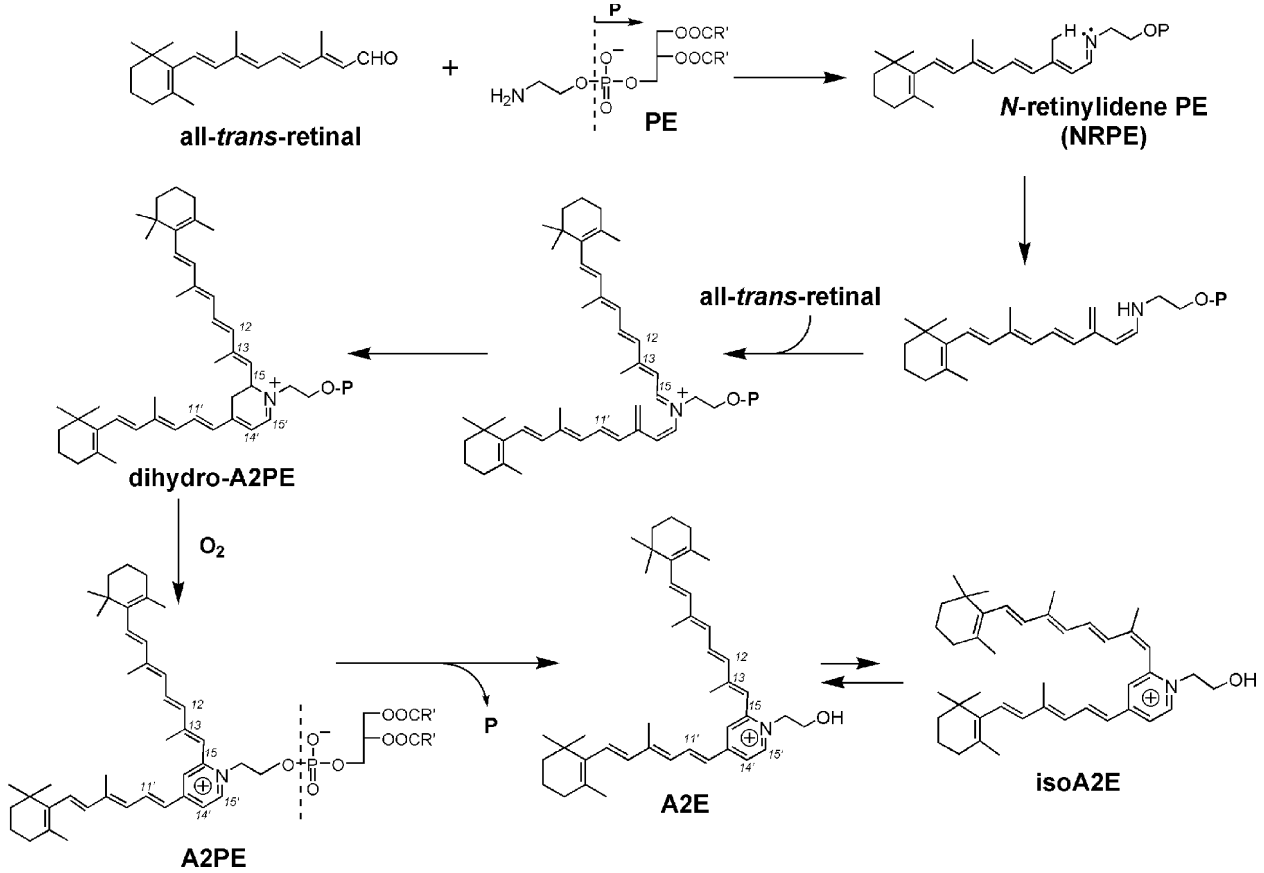

FIGURE 1: Proposed biosynthetic pathway of A2E. All-*trans*-retinal that forms from the photoisomerization of 11-*cis*-retinal reacts with phosphatidylethanolamine (PE) to generate the Schiff base *N*-retinylidene-phosphatidylethanolamine (NRPE). This adduct undergoes a [1,6]-proton tautomerization generating the phosphatidyl analogue of enamine, which reacts with a second molecule of all-*trans*-retinal. Following 6π-electrocyclization, a dihydro-phosphatidyl-pyridinium bisretinoid (dihydro-A2PE) is formed, and after aromatic autoxidation, A2PE is generated. Hydrolysis of the phosphate ester of A2PE yields A2E. The photoisomers A2E and isoA2E exist in photoequilibrium (4:1 ratio).

NRPE is probably the ligand for ABCA4 (ABCR) (*18*−*20*), the photoreceptor-specific ATP-binding cassette transporter that is mutated in recessive Stargardt disease (*21*). We suggested that reaction with a second molecule of all-*trans*-retinal would lead to the formation of a phosphatidyl dihydropyridinium molecule (dihydro-A2PE) that we envisioned would undergo automatic oxidative aromatization to yield A2PE, a phosphatidyl pyridinium bisretinoid. Although the formation of dihydro-A2PE was not, at that time, corroborated, mass spectrometry was utilized to confirm the structure of A2PE (*17*), and experiments demonstrating the release of A2E upon phospholipase D-mediated cleavage of A2PE established A2PE as the immediate precursor of A2E (*13*, *17*).

Since an understanding of A2E biosynthesis is essential to efforts aimed at limiting the formation of this lipofuscin pigment, we have revisited our A2E biogenesis scheme, with the aim of providing evidence for the formation of the dihydropyridinium intermediate, dihydro-A2PE. This transitional compound is of interest to us because it is likely the last intermediate before the stable compound is generated. Dihydropyridinium compounds, such as dihydro-A2PE, are notoriously unstable and undergo automatic oxidative aromatization (*22*); thus, to aid in the identification of dihydro-A2PE in our reaction mixture, we first obtained computer simulations of the UV−visible absorbance spectrum of the compound using TDDFT (*23*, *24*). In subsequent experiments, we sought for evidence of a compound with similar UV−visible spectra and identical mass.

EXPERIMENTAL PROCEDURES

Time-Dependent Density Functional Theory (TDDFT): Geometrical Optimization of Model Compounds. The initial conformers of dihydro-A2E and all-*trans*-retinal dimer-ethanolamine (atRAL dimer-E) were generated by Spartan 02 software (Wavefunction Inc., Irvine, CA) using the Monte Carlo method, and their geometries were optimized with Merck Molecular Force Field (MMFF). Further optimization was achieved using density functional theory at the B3LYP/6-31G* level implemented using a Gaussian 03 software package (*25*). Two stable conformers were found for each of the structures; Cartesian coordinates (Table S1) and stick models (Figures S1 and S2) are presented in Supporting Information. The Gibbs energy differences between the two conformers were 8.50 kJ/mol for dihydro-A2E and 7.54 kJ/mol for atRAL dimer-E *in vacuo*. The conformer populations were calculated by Boltzmann distribution. Since for both dihydro-A2E and atRAL dimer-E the high-energy conformers constituted less than 5% of the total population of conformers, the contribution of the high energy conformers to the overall spectra could be neglected. Accordingly, for the calculations of UV−visible spectra, only the lowest energy conformers were used. The experimental UV−visible absorbance spectra utilized for atRAL dimer-E was that

obtained using a Jasco V530 UV−visible spectrometer with synthesized authentic standard in acetonitrile.

A2E Synthetic Reaction. A mixture of all-*trans*-retinal (300 μg, 2 equiv) and ethanolamine (32 μg, 1 equiv) in ethanol (3 mL) was stirred in the presence of acetic acid (0.3 μL) at room temperature in a capped vial in the dark for the indicated periods of time. For experiments involving synthesis under normal air and deoxygenated conditions, reaction mixtures consisting of all-*trans*-retinal (3 mg), ethanolamine (320 μg), ethanol (6 mL), and acetic acid (3 μL) were either purged or were not purged with argon, before the vessel was closed.

HPLC. An Alliance system (Waters, Corp, Milford, MA) equipped with 2695 Separation Module, 2996 Photodiode Array Detector, and a 2475 Multi λ Fluorescence Detector operating with Empower software was used for HPLC analysis. An Atlantis dC18 column (3 μm, 4.6 × 150 mm, Waters, USA) was employed. A gradient of acetonitrile and water (85% acetonitrile/15% water → 100% acetonitrile for 15 min; 0.8 mL/min) with 0.1% of TFA was used for the mobile phase. Integrated peak areas were determined using Empower software.

Liquid-Chromatography−Mass Spectrometry (LC-MS). LC-MS analysis of the reaction mixture was performed on a Quantum TSQ Discovery mass spectrometer (Thermo Electron, San Jose CA) equipped with a Surveyor autosampler, a Surveyor mass spectrometry pump, and a Surveyor PDA detector. Ten microliters of sample solution was loaded onto the column and eluted isocratically (mobile phase containing 95% acetonitrile, 5% water, and 0.1% formic acid). The column (Atlantis dC18) was heated at 30 °C, and the flow rate was 0.3 mL/min. The mass spectrometer was operated in positive ion mode with spray voltage at 4.0 kV and the ion transfer tube temperature at 300 °C. The Q1 quadrupole scans from *m*/*z* 100 to 1000 with unit resolution.

RESULTS

Calculation of UV−visible absorbance spectra of dihydro-A2PE/dihydro-A2E was performed by time-dependent density functional theory (TDDFT). To aid in the identification of dihydro-A2E in the A2E biomimetic reaction mixture (*12*), we first obtained computer simulations of the UV−visible absorbance spectrum of dihydro-A2E using TDDFT (*23*, *24*). Calculations were based on dihydro-A2E rather than dihydro-A2PE since the phospholipid moiety does not make a contribution to the UV−visible absorbance greater than ~250 nm.

Since the selection of both the functional and the basis set is critical to the UV prediction, we employed two different functionals, namely, B3LYP and BHandHLYP, and two different basis sets, 6-31G* and 6-31+G*, to calculate the UV−visible spectra. The BHandHLYP is a hybrid functional, which combines Beck's half and half (BHandh) exchange functional (*26*) with Lee−Yang-parr (LYP) correlation functional (*27*). As compared to the B3LYP functional, the BHandHLYP functional increases the Hatree−Fock energy exchange contribution. This increase can better handle a situation, which involves electron dissociation (*28*) or excited electronic states of delocalized π-systems (*29*). The 6-31G* basis set is a polarized split-valence basis set that accommodates changes in orbital size and shape in response to a

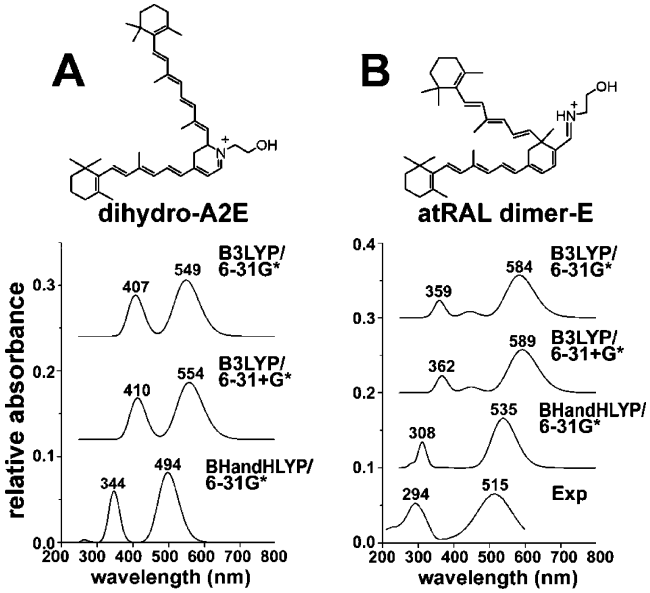

FIGURE 2: Calculated UV−visible absorbance spectra of dihydro-A2E (A) and atRAL dimer-E (B) employing B3LYP and BHandHLYP functionals and 6-31G* and 6-31+G* basis sets within the TDDFT method. An experimentally determined spectrum (Exp) for atRAL dimer-E (A) is also presented.

variation in the electron environment. In the 6-31+G* basis set, the diffuse function (+sign) is added to the heavy atoms in the system. Basis sets with diffuse functions are of value for systems in which electrons may be far from the nucleus. As such, diffuse functions more accurately reflect electron excited states such as occurs with the absorbance of UV and visible light (*30*).

We employed the B3LYP functional across the 6-31G* and 6-31+G* basis sets. However, the addition of the diffuse function did not significantly change the calculated UV−visible absorbance (*31*, *32*). This finding probably reflects the fact that the electron configuration in cations (such as A2E, dihydro-A2PE, and dihydro-A2E; Figure 1) is more compact and as a result can be described by smaller basis sets than are required to describe neutral molecules and anion. Thus to reduce the calculation time, only the 6-31G* basis set was used with the BHandHLYP functional to predict the UV−visible spectra. Accordingly, using the B3LYP functional across 6-31G* and 6-31+G* basis sets and the BHandHLYP functional across the 6-31G* basis set, spectra were calculated for dihydro-A2E (Figure 2). All of the theoretically obtained spectra for dihydro-A2E had similar shapes, and the differences between the two maxima ($\Delta\lambda$) were similar for all of the calculations. Calculation at the BHandHLYP/6-31G* level gave a simulated dihydro-A2E spectrum characterized by absorbance maxima at 494 and 344 nm ($\Delta\lambda$, 150 nm) (Table 1).

As a test of the validity of the functional and basis sets utilized, we also applied these geometrical optimizations to estimate the absorbance spectrum of a compound for which an experimentally derived spectrum was available. For this purpose, we chose atRAL dimer-E, a bis-retinoid RPE lipofuscin pigment, the structure of which has been corroborated by ^{1}H NMR spectroscopy (*16*). Dihydro-A2E (molecular weight, 594) and atRAL dimer-E (Figure 2) have the same molecular weight of 594 but differing numbers of double-bond conjugations (dihydro-A2E: 6 on the long arm,

Table 1: Absorbance Maxima and the Wavelength Difference between Absorbance Peaks ($\Delta\lambda$) Calculated for Dihydro-A2E and atRAL Dimer-E and Presented in Relation to Functional and Basis Sets[a]

	dihydro-A2E			atRAL dimer-E		
	λ_{max} 1	λ_{max} 2	$\Delta\lambda$[b]	λ_{max} 1	λ_{max} 2	$\Delta\lambda$[b]
empirical[c]				294 nm	515 nm	221 nm
B3LYP/ 6-31G*	407 nm	549 nm	142 nm	359 nm 22.1%	584 nm 13.4%	225 nm 1.8%
B3LYP/ 6-31+G*	410 nm	554 nm	144 nm	362 nm 23.1%	589 nm 14.4%	227 nm 2.7%
BHandHLYP/ 6-31G*	344 nm	494 nm	150 nm	308 nm 4.8%	535 nm 3.9%	227 nm 2.7%

[a] For atRAL dimer-E, comparison between the empirically determined spectrum and predicted spectra is presented. The spectra calculated for dihydro-A2E are applicable to dihydro-A2PE (see text for explanation). [b] The difference between λ_{max} 1 and λ_{max} 2. [c] Determined using the synthetic sample.

5 on the short arm; atRAL dimer-E: 7 on the long arm, 4 on short arm); therefore, it was expected that the UV−visible spectra of these compounds would be different. However, given that they have similar polyene structures terminating in β-ionone rings, we reasoned that the geometrical optimizations (functionals and basis sets) providing calculated spectral positions closest to the values observed experimentally for atRAL dimer-E would best estimate the absorbance spectrum of dihydro-A2E. Thus, quantum chemical simulations of UV−visible absorbance spectra of atRAL dimer-E were also performed using TDDFT. The theoretically calculated UV-absorbance spectrum of atRAL dimer-E was compared to the experimentally derived spectrum determined using synthesized atRAL dimer-E.

The comparison between the experimentally derived UV−visible spectrum and TDDFT predicted spectra for atRAL dimer-E is shown in Figure 2. All of the theoretically obtained UV-absorbance spectra for atRAL dimer-E had similar shapes. The peak positions in the B3LYP/6-31G* predicted spectrum were red-shifted relative to the peak positions measured experimentally, a difference which is typical of this theoretical approach (*33*). The B3LYP/6-31+G* predicted spectrum was very similar to the B3LYP/6-31G* predicted spectra, indicating, as discussed above, that the diffuse-function-containing basis set did not have a significant impact on the predicted UV−visible spectra of this structure. The BHandHLYP/6-31G* predicted spectrum was different from the other two predicted spectra, and the peak positions in the BHandHLYP/6-31G* predicted spectrum were closer to the peak positions determined experimentally. A quantitative comparison between the predicted peak position for atRAL dimer-E and the experimental peak position is presented in Table 1. For atRAL dimer-E, the wavelength differences between the two peak positions ($\Delta\lambda$) were very similar for the three predicted spectra ($\Delta\lambda$, 225−227 nm) and were in good agreement with the experimental data ($\Delta\lambda$, 221 nm).

HPLC Analysis of the A2E Biosynthetic Reaction Mixture. Guided by the UV−visible absorbance maxima calculated for dihydro-A2E, we next undertook to detect a compound with similar absorbance in the A2E synthetic reaction mixture of all-*trans*-retinal and ethanolamine. While PE and all-*trans*-

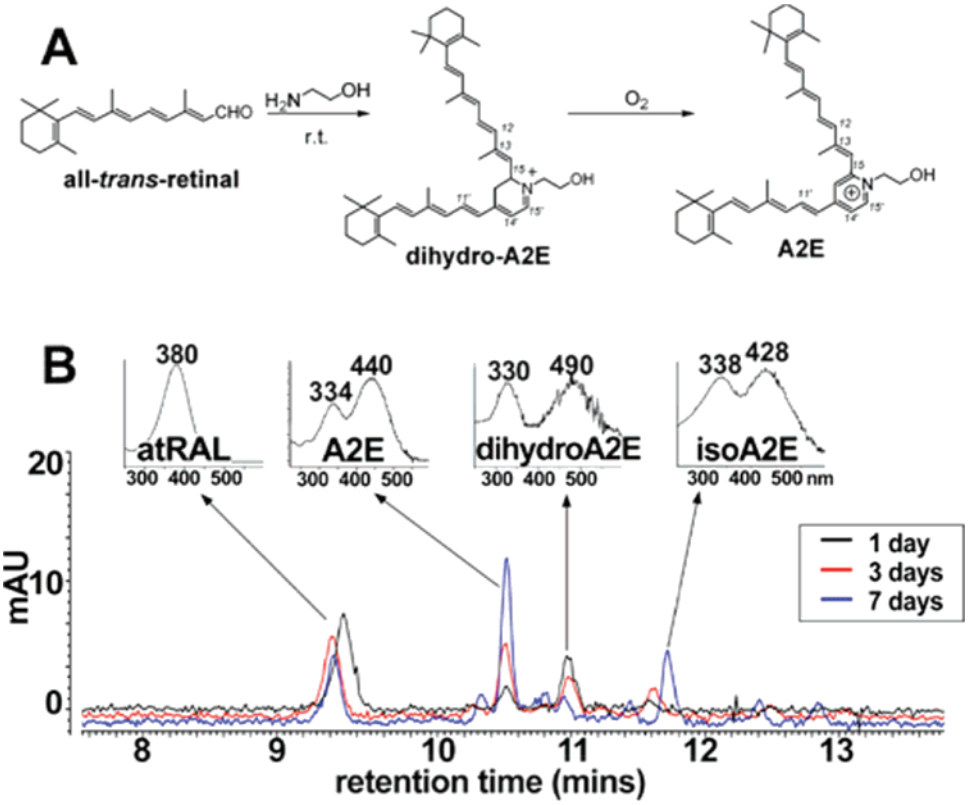

FIGURE 3: Detection of a dihydropyridinium intermediate by HPLC analysis. (A) Biomimetic synthesis of A2E starting from all-*trans*-retinal and ethanolamine with dihydro-A2E as the intermediate; r.t., room temperature. (B) HPLC monitoring of the reaction mixture of all-*trans*-retinal and ethanolamine. The reaction mixture was incubated at room temperature in the dark for 1, 3, or 7 days, and the constituents of the mixture were separated by reverse phase HPLC with monitoring at 430 nm. UV−visible spectra were obtained using a photodiode array detector; atRAL, all-*trans*-retinal.

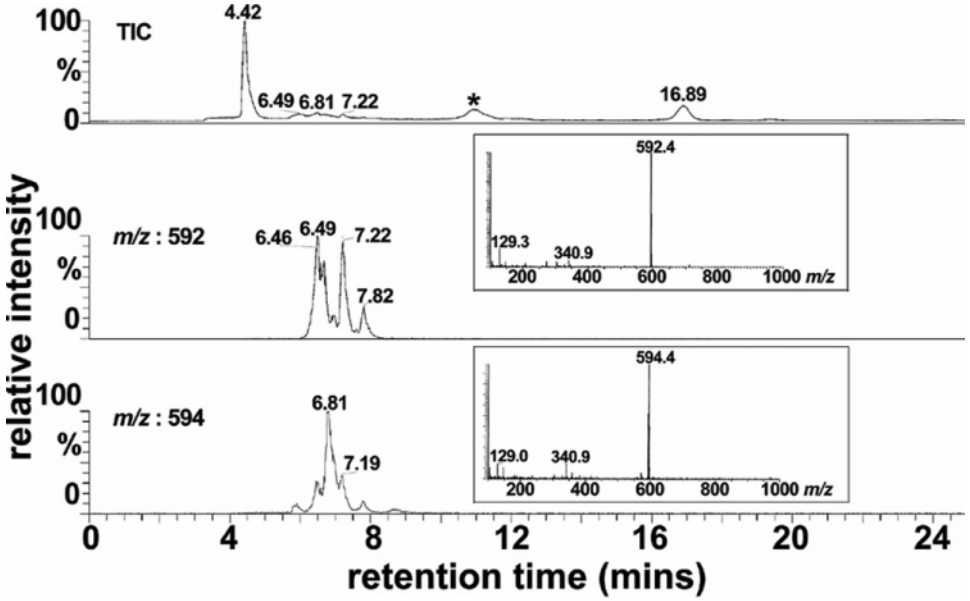

FIGURE 4: LC-MS analysis of the reaction mixture of all-*trans*-retinal and ethanolamine. Full scan acquisition was acquired in ESI mode, recorded as total ion current (TIC), and plotted as a function of retention time in a reversed phase HPLC column (top panel). For selected ion monitoring chromatograms, detection was set for mass to charge (*m*/*z*) ratios of 592 (middle panel) and 594 (bottom panel); *, matrix peak. The multiple peaks in the chromatogram generated with selected ion monitoring at 592 represent A2E isomers; all of these isomers account for the single *m*/*z* peak at 592. The peak at retention time of 7.19 min (selected ion monitoring at 594) is probably an isomer of dihydro-A2E.

retinal are the precursors of A2E *in vivo*, in these experiments, ethanolamine, instead of PE, was used as starting material because condensation of ethanolamine with all-*trans*-retinal is more facile and thus affords more reaction product; moreover, as discussed above, the phospholipid moiety does not contribute to absorbances above ~250 nm. Thus, the findings are applicable to dihydro-A2PE (molecular weight of dihydro-dipalmitoyl-A2PE, 1225). To slow the rate of A2E synthesis, the concentration of starting materials was reduced (1:10) from that typically used for A2E biomimetic synthesis. Monitoring the reaction mixture by reversed phase HPLC using a gradient of acetonitrile and water (with 0.1% TFA) revealed a peak that had a retention time of ~10.9 min, which eluted after A2E and exhibited a UV−visible absorbance spectra characterized by λ_{max} of 490 and 330 nm (Figure 3). The peak height of this fraction diminished at 3 and 7 days of incubation, while the peak height of A2E (λ_{max} of 440 and 334 nm) steadily increased. IsoA2E was also identified on the basis of UV−visible absorbance (λ_{max} of 428 and 338) and was most prominent at 7 days of incubation.

LC-MS Analysis. To obtain the mass of each eluting compound, the 1-day reaction mixture was analyzed by LC-MS using an isocratic gradient of acetonitrile and water with 0.1% formic acid. As shown in Figure 4, the total ion chromatogram revealed signals from three eluting compounds with retention times 6.49−7.22. Operating in selected ion monitoring mode at *m*/*z* 592, two prominent peaks were visible that on the basis of expected mass could be identified as A2E (all-*trans*-A2E, 6.49 min) and isoA2E (C13−C14 *Z*-isomer, 7.22 min). Other minor peaks indicated the presence of additional A2E *cis*-isomers (6.46 and 7.82 min) (*13*). Note that all of these A2E isomers have a weight of 592. With detection at *m*/*z* 594, the expected mass of dihydro-A2E, a major peak eluting between A2E and isoA2E (retention time 6.81 min), was also detectable.

Oxidation of the Dihydro-Pyridinium Intermediate. To test for an oxidation step in the conversion of dihydro-A2PE to A2PE, we next carried out the biomimetic synthesis of A2E under both normal air and deoxygenated (argon) conditions. Again, the starting compounds were all-*trans*-retinal and ethanolamine, and separate reaction mixtures were incubated in parallel to permit independent analysis at 1, 4, and 8 h, and 1, 3, and 7 days. After 1 hour of incubation under normal conditions, a peak attributable to dihydro-A2E (λ_{max} of 490 and 330 nm) was visible without evidence of peaks representing A2E and isoA2E; the dihydro-A2E peak continued to increase in height at 1 and 2 days of incubation but decreased by 3 days (Figure 5). Moreover, under conditions of normal air, peaks attributable to A2E and isoA2E were not apparent until 4 h of incubation, but A2E and isoA2E peak height subsequently increased at 1, 2, and 3 days of incubation. Using peak areas to estimate the relative abundance of the compounds, it was apparent that the amount of dihydro-A2E increased in advance of A2E/isoA2E and up until 2 days of incubation, after which it decreased (Figure 5). However, levels of A2E/isoA2E increased from 4 h until 3 days.

When the synthetic reaction was performed under deoxygenated conditions (Figure 5), the yield of the intermediate compound dihydro-A2E was augmented. Specifically, on the basis of visible peak height and computation of peak area, the intermediate dihydro-A2E increased in amount between 1 and 8 h of reaction and continued to accumulate between 1 and 3 days. By comparison, there was only little evidence of A2E formation between 1 and 8 h of incubation; however, between 1 and 3 days of reaction, a steady increase in A2E peak area was observed (Figure 5).

DISCUSSION

We previously proposed an A2E biosynthetic scheme whereby formation would begin with a reaction between all-

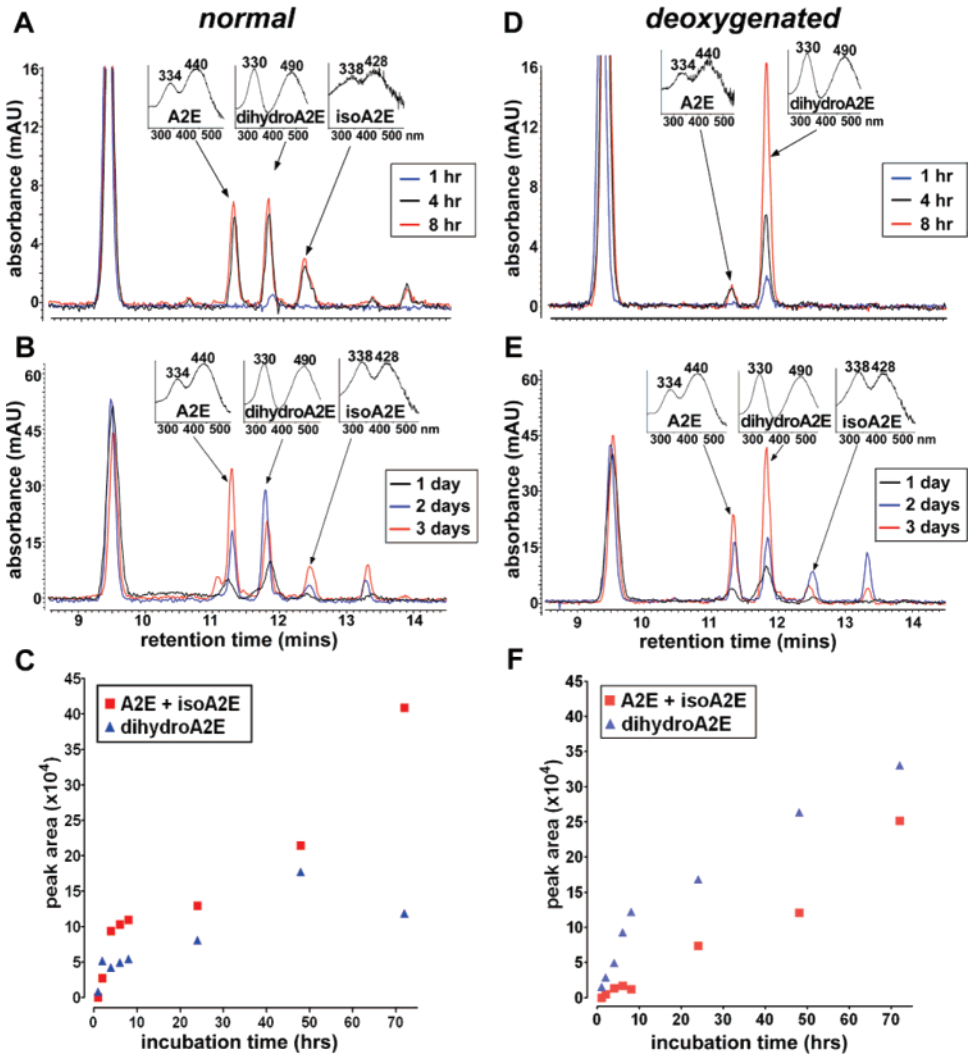

FIGURE 5: Autoxidation step in the A2E synthetic cascade. A2E synthetic reaction under normal air (A and B) and deoxygenated (argon) (D−E) conditions. Starting materials were all-*trans*-retinal and ethanolamine, and reaction mixtures were analyzed by reversed phase HPLC after incubation for 1, 4, and 8 h (A and D) and 1, 2, and 3 days (B and E). Quantitation was performed by integrating chromatographic peak areas (C and F). The major peak eluting at ~9.5 min is all-*trans*-retinal.

trans-retinal and phosphatidylethanolamine (PE) leading to the Schiff base conjugate NRPE that is reported to be the substrate recognized by ABCA4 (ABCR) (*18*−*20*), the photoreceptor-specific ATP-binding cassette transporter, the mutation of which is responsible for recessive Stargardt disease (*21*). NRPE was postulated to undergo a [1,6]-proton tautomerization generating the phosphatidyl analogue of enamine. After reaction with a second molecule of all-*trans*-retinal, we suggested that an iminium salt would form and that following electrocyclization a phosphatidyl dihydropyridinium molecule (dihydro-A2PE) would form. We envisioned that the latter molecule would undergo automatic oxidative aromatization to yield A2PE, a phosphatidyl pyridinium bisretinoid. Mass spectrometry was utilized to confirm the formation of NRPE and A2PE (*17*). Specifically, electrospray ionization (ESI) mass spectrometric analysis of the reaction mixture of dipalmitoyl-l-α-phosphatidylethanolamine and all-*trans*-retinal revealed prominent peaks at *m*/*z* 958.6 and 1222.9 corresponding to the protonated molecular ions of NRPE and A2PE, respectively. Moreover, fast atom bombardment tandem mass spectrometry with collision-induced dissociation mass spectrometric analysis revealed product ions *m*/*z* 551.4 and 408.2 for NRPE, while one product ion at *m*/*z* 672.8 represented the phosphoryl-A2E fragment of A2PE. Additionally, the observation that incubation of A2PE with phospholipase D yields peaks in the HPLC profile that can be identified as A2E and isoA2E on the basis of UV−visible absorbance and retention time confirmed A2PE as the immediate precursor of A2E (*13*, *17*). Several lines of investigation also demonstrated that A2PE forms within photoreceptor outer segments. For instance, the formation of [$^{14}C_2$]-A2PE has been measured in excised whole retinas following [$^{14}C_2$]-ethanolamine incorporation and irradiation to release endogenous all-*trans*-retinal. By mass spectrometric analysis, it has also been shown that A2PE is the orange-colored pigment present in degenerating photoreceptor outer segment debris in Royal College of Surgeon rats (*13*).

The results presented here also now corroborate dihydro-A2PE as an intermediate in the biosynthetic pathway leading to A2PE and then A2E formation. This conclusion is supported by several observations. First, computer simulations of the UV−visible absorbance spectrum of dihydro-A2E using TDDFT, predicted absorbance maxima at 494 and 344 nm. Second, a compound exhibiting absorbance maxima (λ_{max}, 490 and 330 nm) similar to the predicted

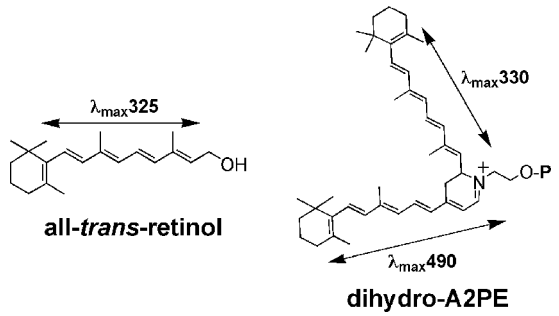

FIGURE 6: Structures of all-*trans*-retinol and dihydro-A2PE. All-*trans*-retinol has an absorbance maximum at 325 nm that reflects an extended conjugation system consisting of a polyene chain of four double bonds with a fifth conjugated olefin in the β-ionone ring. For the bischromophore dihydro-A2PE, an absorbance maximum of 330 nm is generated by the same conjugation system.

maxima was detectable within the A2E synthetic reaction mixture. This compound not only presented with the expected mass (*m*/*z* 594), as determined by LC-MS, it also exhibited an initial accumulation that later slowed and then decreased while A2E levels continued to rise, a pattern typical of intermediate and product, in a biosynthetic reaction.

To ascertain whether an oxidation step was involved in the conversion from dihydro-pyridinium to pyridinium compound, we also carried out the reaction under argon. The final product A2E formed at reduced yield under deoxygenated conditions, while the dihydropyridinium intermediate steadily accumulated. This observation supports the contention that dihydro-A2PE is converted to A2PE by oxidation.

The absorbance spectrum of dihydro-A2E that was calculated by TDDFT (λ_{max}, 494 and 344 nm) agrees well with the spectrum (λ_{max}, 490 and 330 nm) obtained experimentally under HPLC conditions. It is worth noting that with the gradient of acetonitrile and water used for the HPLC mobile phase in these experiments, the concentration of acetonitrile at 11 min (approximate retention time of dihydro-A2E) would be approaching 100%. Acetonitrile is not a highly polar solvent and thus is acceptable for comparing theoretical spectra calculated *in vacuo* with spectra determined experimentally. The 330 nm absorbance maxima of dihydro-A2E/dihydro-A2PE is also consistent with the peak absorbance of all-*trans*-retinol ($\Delta\lambda$, 325 nm). This correlation is significant since the 330 nm absorbance is attributable to the shorter of the two conjugation systems in dihydro-A2E/dihydro-A2PE (Figure 6). This conjugation system consists of five double bonds and terminates in a β-ionone ring; all-*trans*-retinol has the same structure and a maximum absorbance of ~325 nm. Thus, the comparison between dihydro-A2E and all-*trans*-retinol lends further corroboration to the dihydro-A2E absorbance spectrum (λ_{max}, 490 and 330 nm) obtained experimentally. These absorbance maxima can also be assigned to dihydro-A2PE.

In work related to RPE lipofuscin accumulation in *Abcr*$^{-/-}$ mice, a compound with absorbance maxima at 260 and 510 nm has been identified as dihydro-A2PE (A2PE-H_2) (*5*, *34*−*37*). The peak-to-peak interval between these two absorbance maxima is ~250 nm and thus is substantially different from the interval ($\Delta\lambda$, 150 nm) we have calculated and observed experimentally for dihydro-A2E/dihydro-A2PE. In addition, we demonstrate here that the intermediate (the dihydro-pyridinium) in the A2E synthetic pathway that undergoes oxidation to yield A2PE and A2E has absorbance maxima of 330 and 490 nm. Thus, our data do not support the identification of dihydro-A2PE as a 510/260 nm absorbing-species. It is also significant that in the earlier work (*5*, *34*−*37*) a synthesized standard of dihydro-A2PE (A2PE-H_2) was not used to corroborate the identification of the eluting compound.

In the development of novel approaches to the treatment of macular degeneration, attention has been given to approaches that reduce the formation of RPE lipofuscin pigments (*3*−*5*, *8*). Improved understanding of the mode of the genesis of A2E and other RPE lipofuscin compounds could facilitate the introduction of other novel approaches to therapy. In previous studies, we corroborated several steps in the formation of A2E. Here, in work aimed at further elucidation of this multistep pathway, we demonstrate that dihydro-A2PE a compound identifiable by absorbance peaks at 490 and 330 nm is an intermediate in the biosynthetic pathway. An oxidation step is likely involved in the transition from dihydro-A2PE to A2PE since the dihydro-pyridinium bisretinoid intermediate accumulated in the absence of oxygen.

SUPPORTING INFORMATION AVAILABLE

Cartesian coordinates and stick models of conformers used in the calculation of UV−visible absorbances. This material is available free of charge via the Internet at http://pubs.acs.org.

NOTE ADDED AFTER ASAP PUBLICATION

This paper published ASAP on 8/8/07. Additional details were incorporated for the corresponding authors. The revised version was published on 8/13/07.

REFERENCES

1. Katz, M. L., and Redmond, T. M. (2001) Effect of Rpe65 knockout on accumulation of lipofuscin fluorophores in the retinal pigment epithelium, *Invest. Ophthalmol. Visual Sci. 42*, 3023−3030.
2. Kim, S. R., Fishkin, N., Kong, J., Nakanishi, K., Allikmets, R., and Sparrow, J. R. (2004) The Rpe65 Leu450Met variant is associated with reduced levels of the RPE lipofuscin fluorophores A2E and iso-A2E, *Proc. Natl. Acad. Sci. U.S.A. 101*, 11668−11672.
3. Maiti, P., Kong, J., Kim, S. R., Sparrow, J. R., Allikmets, R., and Rando, R. R. (2006) Small molecule RPE65 antagonists limit the visual cycle and prevent lipofuscin formation, *Biochemistry 45*, 852−860.
4. Sieving, P. A., Chaudhry, P., Kondo, M., Provenzano, M., Wu, D., Carlson, T. J., Bush, R. A., and Thompson, D. A. (2001) Inhibition of the visual cycle in vivo by 13-cis retinoic acid protects from light damage and provides a mechanism for night blindness in isotretinoin therapy, *Proc. Natl. Acad. Sci. U.S.A. 98*, 1835−1840.
5. Radu, R. A., Mata, N. L., Nusinowitz, S., Liu, X., Sieving, P. A., and Travis, G. H. (2003) Treatment with isotretinoin inhibits lipofuscin and A2E accumulation in a mouse model of recessive Stargardt's macular degeneration, *Proc. Natl. Acad. Sci. U.S.A. 100*, 4742−4747.
6. Katz, M. L., Drea, C. M., and Robison, W. G., Jr. (1986) Relationship between dietary retinol and lipofuscin in the retinal pigment epithelium, *Mech. Ageing Dev. 35*, 291−305.
7. Katz, M. L., Eldred, G. E., and Robison, W. G., Jr. (1987) Lipofuscin autofluorescence: evidence for vitamin A involvement in the retina, *Mech. Ageing Dev. 39*, 81−90.
8. Radu, R. A., Han, Y., Bui, T. V., Nusinowitz, S., Bok, D., Lichter, J., Widder, K., Travis, G. H., and Mata, N. L. (2005) Reductions in serum vitamin A arrest accumulation of toxic retinal fluoro-

phores: a potential therapy for treatment of lipofuscin-based retinal diseases, *Invest. Ophthalmol. Visual Sci. 46*, 4393−4401.
9. Eldred, G. E., and Lasky, M. R. (1993) Retinal age pigments generated by self-assembling lysosomotropic detergents, *Nature 361*, 724−726.
10. Eldred, G. E., and Katz, M. L. (1988) Fluorophores of the human retinal pigment epithelium: separation and spectral characterization, *Exp. Eye Res. 47*, 71−86.
11. Sakai, N., Decatur, J., Nakanishi, K., and Eldred, G. E. (1996) Ocular age pigment "A2E": an unprecedented pyridinium bisretinoid, *J. Am. Chem. Soc. 118*, 1559−1560.
12. Parish, C. A., Hashimoto, M., Nakanishi, K., Dillon, J., and Sparrow, J. R. (1998) Isolation and one-step preparation of A2E and iso-A2E, fluorophores from human retinal pigment epithelium, *Proc. Natl. Acad. Sci. U.S.A. 95*, 14609−14613.
13. Ben-Shabat, S., Parish, C. A., Vollmer, H. R., Itagaki, Y., Fishkin, N., Nakanishi, K., and Sparrow, J. R. (2002) Biosynthetic studies of A2E, a major fluorophore of RPE lipofuscin, *J. Biol. Chem. 277*, 7183−7190.
14. Ren, R. F., Sakai, N., and Nakanishi, K. (1997) Total synthesis of the ocular age pigment A2E: a convergent pathway, *J. Am. Chem. Soc. 119*, 3619−3620.
15. Fishkin, N., Pescitelli, G., Sparrow, J. R., Nakanishi, K., and Berova, N. (2004) Absolute configurational determination of an all-*trans*-retinal dimer isolated from photoreceptor outer segments, *Chirality 16*, 637−641.
16. Fishkin, N., Sparrow, J. R., Allikmets, R., and Nakanishi, K. (2005) Isolation and characterization of a retinal pigment epithelial cell fluorophore: an all-trans-retinal dimer conjugate, *Proc. Natl. Acad. Sci. U.S.A. 102*, 7091−7096.
17. Liu, J., Itagaki, Y., Ben-Shabat, S., Nakanishi, K., and Sparrow, J. R. (2000) The biosynthesis of A2E, a fluorophore of aging retina, involves the formation of the precursor, A2-PE, in the photoreceptor outer segment membrane, *J. Biol. Chem. 275*, 29354−29360.
18. Weng, J., Mata, N. L., Azarian, S. M., Tzekov, R. T., Birch, D. G., and Travis, G. H. (1999) Insights into the function of Rim protein in photoreceptors and etiology of Stargardt's disease from the phenotype in abcr knockout mice, *Cell 98*, 13−23.
19. Sun, H., Molday, R. S., and Nathans, J. (1999) Retinal stimulates ATP hydrolysis by purified and reconstituted ABCR, the photoreceptor-specific ATP-binding cassette transporter responsible for Stargardt disease, *J. Biol. Chem. 274*, 8269−8281.
20. Sun, H., and Nathans, J. (1997) Stargardt's ABCR is localized to the disc membrane of retinal rod outer segments, *Nat. Genet. 17*, 15−16.
21. Allikmets, R., Singh, N., Sun, H., Shroyer, N. F., Hutchinson, A., Chidambaram, A., Gerrard, B., Baird, L., Stauffer, D., Peiffer, A., Rattner, A., Smallwood, P., Li, Y., Anderson, K. L., Lewis, R. A., Nathans, J., Leppert, M., Dean, M., and Lupski, J. R. (1997) A photoreceptor cell-specific ATP-binding transporter gene (ABCR) is mutated in recessive Stargardt macular dystrophy, *Nat. Genet. 15*, 236−246.
22. Dalvis, D., Zhao, Z., and Castagnoli, N. (1992) Characterization of an unexpected product from a monoamine oxidase B generated 2,3-dihydropyridinium species, *J. Org. Chem. 57*, 7321−7324.
23. Preat, J., Jacquemin, D., Wathelet, V., Andre, J. M., and Perpete, E. A. (2006) TD-DFT investigation of the UV spectra of pyranone derivatives, *J. Phys. Chem. A 110*, 8144−8150.
24. Casida, M. E., Jamorski, C., Casida, K. C., and Salahub, D. R. (1998) Molecular excitation energies to high-lying bound states from time-dependent density-functional response theory: Characterization and correction of the time-dependent local density approximation ionization threshold, *J. Chem. Phys 108*, 4439−4449.
25. Frisch, M. J., Trucks, G. W., Schlegel, H. B., Scuseria, G. E., Robb, M. A., Cheeseman, J. R., Montgomery, J. A., Jr., Vreven, T., Kudin, K. N., Burant, J. C., Millam, J. M., Iyengar, S. S., Tomasi, J., Barone, V., Mennucci, B., Cossi, M., Scalmani, G., Rega, N., Petersson, G. A., Nakatsuji, H., Hada, M., Ehara, M., Toyota, K., Fukuda, R., Hasegawa, J., Ishida, M., Nakajima, T., Honda, Y., Kitao, O., Nakai, H., Klene, M., Li, X., Knox, J. E., Hratchian, H. P., Cross, J. B., Bakken, V., Adamo, C., Jaramillo, J., Gomperts, R., Stratmann, R. E., Yazyev, O., Austin, A. J., Cammi, R., Pomelli, C., Ochterski, J. W., Ayala, P. Y., Morokuma, K., Voth, G. A., Salvador, P., Dannenberg, J. J., Zakrzewski, V. G., Dapprich, S., Daniels, A. D., Strain, M. C., Farkas, O., Malick, D. K., Rabuck, A. D., Raghavachari, K., Foresman, J. B., Ortiz, J. V., Cui, Q., Baboul, A. G., Clifford, S., Cioslowski, J., Stefanov, B. B., Liu, G., Liashenko, A., Piskorz, P., Komaromi, I., Martin, R. L., Fox, D. J., Keith, T., Al-Laham, M. A., Peng, C. Y., Nanayakkara, A., Challacombe, M., Gill, P. M. W., Johnson, B., Chen, W., Wong, M. W., Gonzalez, C., Pople, J. A. (2004) *Gaussian 03*, revision C.02, Gaussian, Inc., Wallingford, CT.
26. Becke, A. D. (1993) A new mixing of Hartree-Fock and local density-functional theories, *J. Chem. Phys. 98*, 1372−1377.
27. Lee, C., Yang, W., and Parr, R. G. (1988) Development of the Colle-Salvetti correlation-energy formula into a functional of the electron density, *Phys. Rev. B 37*, 785−789.
28. Zhang, Y., and Yang, W. (1998) A challenge for density functional: self-interaction error increases for systems with a noninteger number of electrons, *J. Chem. Phys. 109*, 2604−2608.
29. Polavarapu, P. L., He, J., Crassous, J., and Ruud, K. (2005) Absolute configuration of C76 from optical rotatory dispersion, *ChemPhysChem 6*, 2535−2540.
30. Preat, J., Jacquemin, D., and Perpete, E. A. (2005) Theoretical investigations of the UV spectra of coumarin derivatives, *Chem. Phys. Lett. 415*, 20−24.
31. Hirata, S., Lee, T. J., and Head-Gordon, M. (1999) Time-dependent density functional study on the electronic excitation energies of polycyclic aromatic hydrocarbon radical cations of naphthalene, anthracene, pyrene and perylene, *J. Chem. Phys. 111*, 8904−8912.
32. Nemykin, V. N., and Basu, P. (2003) Comparative theoretical investigation of the vertical excitation energies and the electronic structure of $[Mo^{V}0Cl_4]^{-}$: influence of basis set and geometry, *Inorg. Chem. 42*, 4046−4056.
33. Cavillot, V., and Champagne, B. (2005) Simulation of UV/visible absorption spectra of (a-diimine)nickel(II) catalysts by time-dependent density functional theory, *Int. J. Quantum Chem. 101*, 840−848.
34. Mata, N. L., Tzekov, R. T., Liu, X., Weng, J., Birch, D. G., and Travis, G. H. (2001) Delayed dark adaptation and lipofuscin accumulation in abcr+/− mice: implications for involvement of *ABCR* in age-related macular degeneration, *Invest. Ophthalmol. Visual Sci. 42*, 1685−1690.
35. Mata, N. L., Weng, J., and Travis, G. H. (2000) Biosynthesis of a major lipofuscin fluorophore in mice and humans with ABCR-mediated retinal and macular degeneration, *Proc. Natl. Acad. Sci. U.S.A. 97*, 7154−7159.
36. Radu, R. A., Mata, N. L., Bagla, A., and Travis, G. H. (2004) Light exposure stimulates formation of A2E oxiranes in a mouse model of Stargardt's macular degeneration, *Proc. Natl. Acad. Sci. U.S.A. 101*, 5928−5933.
37. Bui, T. V., Han, Y., Radu, R. A., Travis, G. H., and Mata, N. L. (2006) Characterization of native retinal fluorophores involved in biosynthesis of A2E and lipofuscin-associated retinopathies, *J. Biol. Chem. 281*, 18112−18119.

BI7009635